Optics Letters

Miniature multicore optical fiber vibration sensor

JOEL VILLATORO,[1,2,*] ENRIQUE ANTONIO-LOPEZ,[3] AXEL SCHÜLZGEN,[3] AND RODRIGO AMEZCUA-CORREA[3]

[1]Department of Communications Engineering, Escuela de Ingeniería de Bilbao, University of the Basque Country (UPV/EHU), Alameda de Urquijo s/n, E-48013 Bilbao, Spain
[2]IKERBASQUE—Basque Foundation for Science, E-48011 Bilbao, Spain
[3]CREOL, The College of Optics & Photonics, University of Central Florida, P.O. Box 162700, Orlando, Florida 32816-2700, USA
*Corresponding author: agustinjoel.villatoro@ehu.eus

Received 15 March 2017; revised 26 April 2017; accepted 2 May 2017; posted 3 May 2017 (Doc. ID 290714); published 12 May 2017

We demonstrate a compact and versatile interferometric vibration sensor that operates in reflection mode. To build the device, a short segment of symmetric strongly coupled multicore optical fiber (MCF) is fusion spliced to a single-mode optical fiber (SMF). One end of the MCF segment is cleaved and placed in a cantilever position. Due to the SMF-MCF configuration, only two supermodes are excited in the MCF. Vibrations induce cyclic bending of the MCF cantilever which results in periodic oscillations of the reflected interference spectrum. In our device, the MCF itself is the inertial mass. The frequency range where our device is sensitive can be easily tailored from a few hertz to several kilohertz through the cantilever dimensions.

OCIS codes: (060.2370) Fiber optics sensors; (060.4005) Microstructured fibers; (280.4788) Optical sensing and sensors.

https://doi.org/10.1364/OL.42.002022

Vibration sensors have a large and diverse number of applications. Such sensors are vital to monitoring seismic events or the structural health of machinery and civil infrastructures [1]. Vibration sensors are also important in oil and gas exploration [2]. Different applications and the environmental conditions require tailored vibration sensor characteristics. For example, to monitor earthquakes or volcanic eruptions, as well as civil infrastructures (buildings, bridges, etc.), vibration sensors that respond to low frequencies (below a few tens of hertz) are necessary [3]. On the other hand, monitoring the health status of machines demands vibration sensors that respond to medium or high frequencies (from a few hundred hertz to several kilohertz) [4].

Currently, there exists a large variety of vibration sensors (also called accelerometers). However, the interest in fiber optic vibration sensors has grown considerably in the last years. This interest is triggered by the distinct advantages that fiber optic sensors offer, including immunity to electromagnetic interference, remote operation, multiplexing capability, and high sensitivity. So far, a number of device approaches to fiber optic vibration sensors have been reported [1,2]. Since lightweight optical fibers are fairly insensitive to vibrations, the majority of vibration sensors feature a much heavier test mass that is coupled to the fiber and results in a bulky sensor device. Vibrations move the test mass periodically and, consequently, the optical fiber experiences cyclic strain or displacements. The latter two effects cause changes in the intensity, phase, or wavelength of the guided light. As a result, different types of fiber optic sensors can be applied to monitoring vibrations. Intensity-modulated vibration sensors are the simplest ones, but their accuracy is poor [5–10]. Interferometric vibration sensors are highly sensitive but, in general, they tend to be complex and, hence, impractical [11–15]. Vibration sensors based on fiber Bragg grating (FBG) technology are the most advanced ones and have reached commercial level [16–20]. The main disadvantage of FBG vibration sensors is their high cost, as picometer-resolution systems are required to interrogate them.

Here, we introduce a miniature interferometric vibration sensor based on strongly coupled multicore optical fiber (MCF); see Fig. 1. One end of a short segment of MCF is fusion spliced to a single-mode fiber (SMF). The other end of the MCF is cleaved and, subsequently, a short segment of capillary tube is spliced to the MCF. The structure is placed in a cantilever position, as shown in Fig. 1. Due to the axial symmetry of the SMF-MCF structure, only two supermodes are excited in the MCF when light is launched through the SMF, and these supermodes interfere in a very predictable manner [21–25]. In

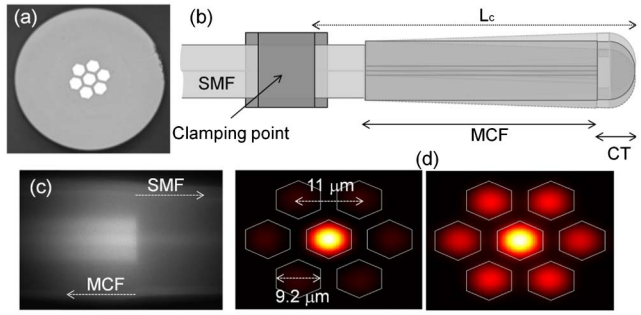

Fig. 1. (a) Micrograph of the MCF used in the experiments. (b) Illustration of the sensor. Lc is the cantilever length and CT means capillary tube. (c) Micrograph of the SMF-MCF junction. (d) Simulated profiles, at 1550 nm, of the two supermodes that participate in the interference.

our configuration, the MCF is sensitive to vibrations, as this supermode interference is highly sensitive to small bending angles [24]. Vibrations bend cyclically the MCF and induce periodic oscillations of the reflected interference spectrum. In our configuration, the MCF functions not only as the light waveguide, but it also plays the role of the test mass. We will demonstrate that changing the dimensions of the cantilever allows us to tailor the operating frequency range of our sensor from a few hertz to several kilohertz.

The MCF used to fabricate our devices has seven identical cores made of Ge-doped silica. The core arrangement, dimensions of the cores, and the separation between them are indicated in Fig. 1. The outer diameter of the MCF is ca 140 μm. The particular feature of our MCF is that the numerical aperture (NA) of each core is 0.14 (at 1550 nm), well matched to the NA of a conventional SMF. Due to this feature, the coupling between the MCF and the SMF is highly efficient, and the insertion loss of our devices is low, typically around 0.1 dB. The fabrication of the structure, as shown in Fig. 1, is straightforward. A segment of the aforementioned MCF is fusion spliced with SMF with a splicing machine (in our case, we used a Fujikura 100P+). The default programs installed in the machine for splicing standard optical fibers were used. Then, the MCF is cleaved to a desirable length; in our case, the typical lengths were between 5 mm and 6 cm, as other lengths were found to be impractical for our applications. The cleaved end of the MCF acts as a low-reflectivity mirror; however, a metal can also be deposited on the MCF end if high reflectivity is required. To protect the MCF end (i.e., the mirror), a short segment (~4 mm) of the capillary tube with an internal/external diameter of 50/130 μm was fusion spliced to the MCF. A proper arc discharge was applied to the capillary tube to seal it completely.

Although our MCF supports seven supermodes [21], only two supermodes are excited and guided in the MCF segment due to the excitation symmetry of the SMF-MCF connection. Figure 1 shows the profiles of these two supermodes. The simulations were calculated for 1550 nm with the finite difference method using commercial waveguide software (FimmWave by Photon Design). The supermodes interfere during propagation in the MCF; light is reflected from the cleaved end of the MCF and coupled back into the SMF core. The interference between the supermodes results in spectrally periodic coupling of the reflected power back into the SMF core. The supermodes excited in the MCF have different propagation constants which can be denoted by β_1 and β_2. During propagation through the MCF, a phase difference of $\Delta\phi = 2L_f(\beta_1 - \beta_2)$, where L_f is the length of MCF, is acquired between the two supermodes. Since this phase difference depends on the wavelength, the reflected spectrum of the SMF-MCF structure is expected to feature maxima and minima related to constructive and destructive supermode interference at the recoupling point into the SMF core, respectively. We will see that if the segment of MCF is short, the spectral period of the interference pattern is large, and vice versa.

It has been demonstrated that supermode interference is highly sensitive to bending [24,25]. Thus, if the MCF is placed in a cantilever position, as shown in Fig. 1, a periodic shift to the reflected spectrum can be induced. Such a periodic shift can be monitored with high accuracy. Therefore, simple and accurate vibration sensors can be implemented with the configuration shown here.

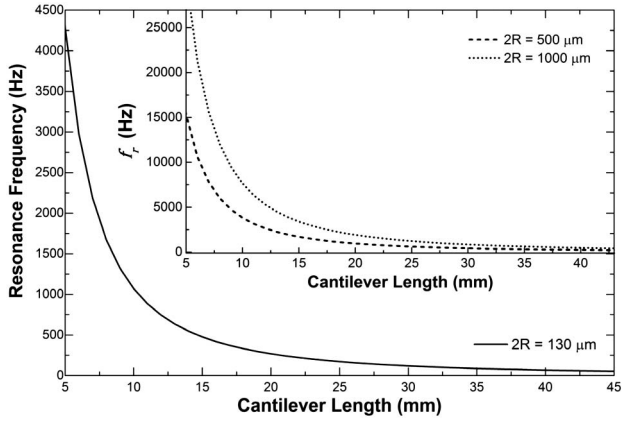

Fig. 2. Theoretical resonance frequency as a function of the cantilever length. Three possible diameters of the cantilever were considered.

The resonance frequency (f_r) of our cantilever can be calculated with formulas provided in the literature as, for example, with those provided in [5,14], or [26], which state that

$$f_r = \frac{F_0}{4\pi}\left(\frac{R}{L_c^2}\right)\sqrt{E/\rho}, \tag{1}$$

where F_0 is a constant, which is ≈3.52 for the zeroth-order vibration mode of the cantilever; R can be taken as the radius of the MCF; L_c is the length of the cantilever, i.e., the distance from the clamping point to the end of the sealed capillary [see Fig. 1(b)]; E and ρ are, respectively, the Young's modulus and the mass density of the cantilever. As the latter is made of glass, E and ρ can be considered as those of silica which are well known.

In Fig. 2, we show the theoretical resonance frequency of the cantilever for different values of R and L_c. Note that, in theory, the resonance frequency of our sensors can be adjusted from around 50 Hz to more than 25 kHz. In a practical situation, such a broad range can be achieved, as the MCF diameter can be controlled during the fiber fabrication. Moreover, the cantilever can be protected with thick capillary tubes, and the cantilever length can be easily adjusted.

We fabricated several samples and interrogated them by launching light from a superluminescent diode with a peak emission at 1550 nm. The reflected light was analyzed with a miniature spectrometer (I-MON512-USB, Ibsen Photonics) connected to a personal computer. Figure 3 shows the reflected spectra of two MCF interferometers, where L_f was 19 or 40 mm. We noticed that the short segment of a capillary tube spliced to the MCF did not distort the reflected spectra.

To monitor vibrations with our devices, it is crucial to track the cyclic shifts of the interference patterns with high speed and accuracy. To do so, we used the center of gravity (COG) algorithm installed in our spectrometer. The COG algorithm is fast and allows us to find and track the maximum wavelength of a peak with high accuracy, even if it is ultrabroad. According to the COG algorithm, the peak wavelength (λ_p) of the broad peak shown in Fig. 3 is simply [27]

$$\lambda_p = \frac{\sum_1^m I_i\lambda_i}{\sum_1^m I_i}. \tag{2}$$

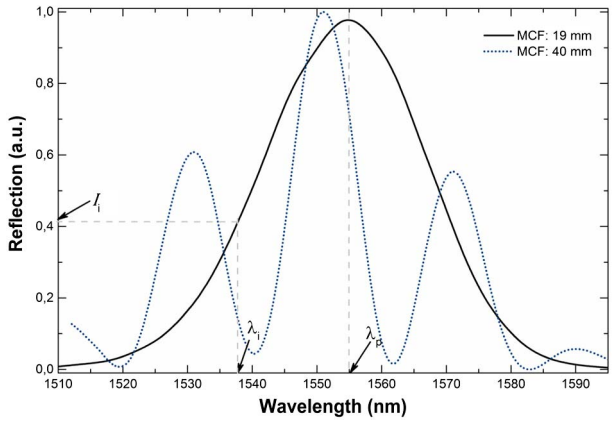

Fig. 3. Normalized reflection spectra of two devices fabricated with 19 and 40 mm of MCF. In the 19 mm long device, λ_p is the peak wavelength, and I_i is the reflection intensity at the wavelength λ_i.

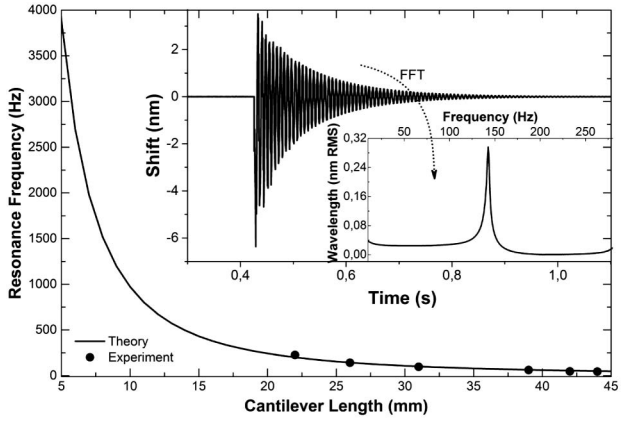

Fig. 4. Resonance frequency versus the length of the cantilever. The dots are experimental values, and the continuous line is the theoretical curve. The inset plots show the shift versus time, and the FFT. In all cases, an interferometer fabricated with 19 mm of MCF was used.

In Eq. (2), I_i is the reflected intensity at the wavelength λ_i, and m is the number of points in which the broad peak is fragmented. In our case, the initial and final wavelengths (λ_1 and λ_m) were those located at the minima of the spectrum. The number of points, or m, to calculate λ_p were always less than 512, as this was the number of pixels that composed the detector of our spectrometer.

A 19 mm-long MCF interferometer protected with a capillary tube was placed in a cantilever position, as shown in Fig. 1. The initial cantilever length was 22 mm. It important to point out that the clamping point was outside the MCF because the MCF in sensitive to local pressure. To determine the resonance frequency of the cantilever, it was made to oscillate freely. To do so, we blew air to the cantilever. The position of the peak wavelength (λ_p) as a function of time was recorded; the frequency of the oscillation was calculated by means of the fast Fourier transform (FFT). The clamping point was changed, and the resonance frequency of the new cantilever was measured. The results of our experiments are summarized in Fig. 4, where we show the shift of the interference pattern as a function of time, the FFT, and the resonance frequency observed for different lengths of the cantilever. It is important to mention here that all the segments that composed the cantilever were without any coating. In addition, the orientation of the MCF cores was arbitrary. We observed that interferometers built with longer lengths of MCF gave essentially similar resonance versus cantilever length graphs as those plotted in Fig. 4.

To further characterize our MCF interferometer as a vibration sensor, we placed it close to a loudspeaker (model GF0776MX, from Amaoto Industrial Co.), as shown in the inset of Fig. 5. For these experiments, the cantilever length was 44 mm. (L_f was 19 mm, and the MCF was also protected with a capillary tube.) The acoustic waves generated by the loudspeaker induced minute periodic bending to the MCF, hence periodic shifts to the reflected interference pattern. The frequency of the loudspeaker was changed with a function generator (model 33120A, from Hewlett-Packard). For all frequencies, the driving voltage was 10 V. The inset of Fig. 5 shows the observed FFTs for two frequencies of the loudspeaker. The figure also shows the frequency we measured with our MCF interferometer and the frequency of the loudspeaker which was controlled by the function generator. The calibration gave us the following expression: $F_m = 0,99986F_i$, where F_m and F_i, respectively, are the measured and the input frequency. The frequency range we could measure was from 40 to 760 Hz. We believe that this is not a limitation of our device. According to the manufacturer, the resonance frequency of the loudspeaker is around 310 Hz. Thus, at frequencies outside the resonance frequency the acoustic pressure is too weak to bend the MCF.

It is important to mention here that our MCF interferometer is sensitive to temperature. In fact, it can operate up to 1000°C, as demonstrated in a previous publication [21]. Temperature causes a shift of the interference pattern. However, in our case, we do not monitor such a shift but the period of the shift. In this manner, temperature does not affect our measurements.

We also investigated the response of our device to different vibration amplitudes. To do so, we placed the aforementioned loudspeaker at 3 cm from the cantilever (or MCF) and changed

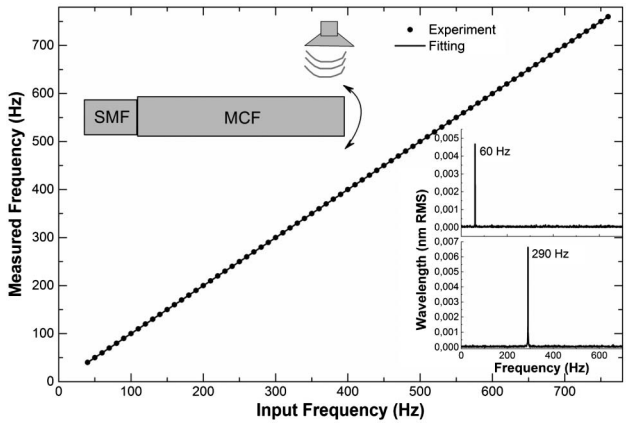

Fig. 5. Measured frequency with our MCF interferometer versus the input frequency of the speaker. The dots are experimental values, and the continuous line is a fitting to the data. The inset drawing shows an illustration of the experimental setup. The inset plots show the FFT at 60 and 290 Hz. In all cases, L_f was 19 mm.

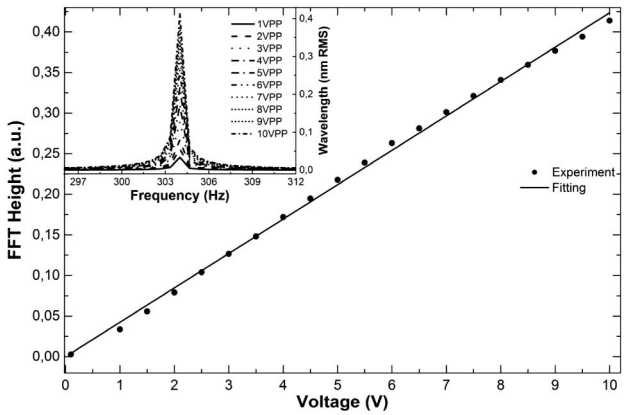

Fig. 6. FFT amplitude as a function of the driving voltage applied to the loudspeaker. The inset graphs show the FFTs at different driving voltages. In all cases, L_f was 19 mm.

the driving voltage of the speaker from 1 to 10 V (the maximum possible voltage with our function generator). The frequency of the speaker was kept fixed at 304 Hz, i.e., close to the speaker resonance frequency. Figure 6 summarizes our results. It can be seen that as the driving voltage of the loudspeaker increases, the height (amplitude) of the FFT increases. The calibration gave us the following expression: FFT amplitude $= 0,04236V$, where V is the driving voltage.

In conclusion, we have demonstrated a simple and compact interferometric vibration sensor based on strongly coupled MCFs. Our device consists of a short segment of MCF fusion spliced at the distal end of a single-mode fiber. The fabrication of our device takes a few minutes; it is reproducible and inexpensive. Due to the features of the MCF used and the excitation conditions, only two supermodes participate in the interference. To monitor vibrations, we placed our MCF interferometers in a cantilever position. Vibrations cause cyclic bending to the MCF which is detected as a periodic oscillation of the interference pattern in the reflection spectra. We demonstrated that the resonance frequency of our sensors can be easily tuned from a few hertz to several kilohertz. Thus, we believe that our device can be useful in diverse applications.

Funding. Federación Española de Enfermedades Raras (FEDER); Gobierno Vasco/Eusko Jaurlaritza (IT933-16 ELKARTEK); Ministerio de Economía y Competitividad (MINECO), Spain (TEC2015-638263-C03-1-R).

REFERENCES

1. T. K. Gangopadhyay, Sens. Actuators A **113**, 20 (2004).
2. X. Qiao, Z. Shao, W. Bao, and Q. Rong, Sensors **17**, 429 (2017).
3. P. F. da Costa Antunes, H. F. T. Lima, and N. J. Alberto, IEEE Sens. J. **9**, 1347 (2009).
4. R. P. Linessio, K. de Morais Sousa, T. da Silva, C. A. Bavastri, P. F. da Costa Antunes, and J. C. C. da Silva, IEEE Sens. J. **16**, 8075 (2016).
5. J. Kalenik and R. Pająk, Sens. Actuators A **68**, 350 (1998).
6. T. Guo, L. Shao, H.-Y. Tam, P. A. Krug, and J. Albert, Opt. Express **17**, 20651 (2009).
7. B. Xu, Y. Li, M. Sun, Z. W. Zhang, X. Y. Dong, Z. X. Zhang, and S. Z. Jin, Opt. Lett. **37**, 4768 (2012).
8. P. Lu, Y. Xu, F. Baset, X. Bao, and R. Bhardwaj, Appl. Phys. Lett. **103**, 211113 (2013).
9. Z. Wang, W. Zhang, J. Han, W. Huang, and F. Li, J. Lightwave Technol. **32**, 4208 (2014).
10. Y. Guozhen, L. Yongqian, and Y. Zhi, Opt. Fiber Technol. **29**, 53 (2016).
11. B. Dong, B. Zhang, J. Ng, Y. Wang, and C. Yu, IEEE Photon. Technol. Lett. **27**, 2234 (2011).
12. F. Yang, W. Jin, H. L. Ho, F. Wang, W. Liu, L. Ma, and Y. Hu, Opt. Express **21**, 15514 (2013).
13. T. Zhang, Y. Zhao, D. Wei, and J. Pan, IEEE Photon. Technol. Lett. **26**, 2361 (2014).
14. X. Wu, X. Wang, S. Li, S. Huang, Q. Ge, and B. Yu, IEEE Photon. Technol. Lett. **27**, 1632 (2015).
15. D. Pawar, C. N. Rao, R. K. Choubey, and S. N. Kale, Appl. Phys. Lett. **108**, 041912 (2016).
16. T. A. Berkoff and A. D. Kersey, IEEE Photon. Technol. Lett. **8**, 1677 (1996).
17. M. D. Todd, G. A. Johnson, B. A. Althouse, and S. T. Vohra, IEEE Photon. Technol. Lett. **10**, 1605 (1998).
18. A. Laudati, F. Mennella, M. Giordano, G. D'Altrui, C. C. Tassini, and A. Cusano, IEEE Photon. Technol. Lett. **19**, 1991 (2007).
19. Y. Weng, X. Qiao, T. Guo, M. Hu, Z. Feng, R. Wang, and J. Zhang, IEEE Sens. J. **12**, 800 (2011).
20. T. Li, Y. Tan, and Z. Zhou, Sensors **16**, 547 (2016).
21. J. E. Antonio-Lopez, S. Eznaveh, P. LiKamWa, A. Schülzgen, and R. Amezcua-Correa, Opt. Lett. **39**, 4309 (2014).
22. A. Van Newkirk, E. Antonio-Lopez, G. Salceda-Delgado, R. Amezcua-Correa, and A. Schülzgen, Opt. Lett. **39**, 4812 (2014).
23. G. Salceda-Delgado, A. Van Newkirk, J. E. Antonio-Lopez, A. Schülzgen, A. Martinez-Rios, and R. Amezcua-Correa, Opt. Lett. **40**, 1468 (2015).
24. J. Villatoro, A. Van Newkirk, J. E. Antonio-Lopez, J. Zubia, A. Schülzgen, and R. Amezcua-Correa, Opt. Lett. **41**, 832 (2016).
25. A. Van Newkirk, J. E. Antonio-Lopez, A. Velazquez-Benitez, J. Albert, R. Amezcua-Correa, and A. Schülzgen, Opt. Lett. **40**, 5188 (2015).
26. X. Liu, M. J. Cobb, Y. Chen, M. B. Kimmey, and X. Li, Opt. Lett. **29**, 1763 (2004).
27. A. Ezbiri, S. E. Kanellopoulos, and V. A. Handerek, Opt. Commun. **150**, 43 (1998).